Available online at www.sciencedirect.com

ScienceDirect

Biochimica et Biophysica Acta 1768 (2007) 1070–1082

Biochimica et Biophysica Acta BBA

www.elsevier.com/locate/bbamem

Structure and conformation of the disulfide bond in dimeric lung surfactant peptides SP-B_{1-25} and SP-B_{8-25}

Nilanjana Biswas [a], Alan J. Waring [b,c], Frans J. Walther [c], Richard A. Dluhy [a,*]

[a] *Department of Chemistry, University of Georgia, Athens, GA 30602-2556, USA*

[b] *Department of Medicine, Division of Infectious Diseases, Center for the Health Sciences, UCLA, 10833 Le Conte Avenue, Los Angeles, CA 90095, USA*

[c] *Department of Pediatrics, LA BioMed at Harbor-UCLA Medical Center, 1124 West Carson Street, Building F-5 South, Torrance, CA 90502, USA*

Received 12 July 2006; received in revised form 15 January 2007; accepted 24 January 2007
Available online 6 February 2007

Abstract

Raman spectroscopy was used to determine the conformation of the disulfide linkage between cysteine residues in the homodimeric construct of the N-terminal alpha helical domain of surfactant protein B (dSP-B_{1-25}). The conformation of the disulfide bond between cysteine residues in position 8 of the homodimer of dSP-B_{1-25} was compared with that of a truncated homodimer (dSP-B_{8-25}) of the peptide having a disulfide linkage at the same position in the alpha helix. Temperature-dependent Raman spectra of the S–S stretching region centered at ~500 cm^{-1} indicated a stable, although highly strained disulfide conformation with a χ(CS–SC) dihedral angle of ±10° for the dSP-B_{1-25} dimer. In contrast, the truncated dimer dSP-B_{8-25} exhibited a series of disulfide conformations with the χ(CS–SC) dihedral angle taking on values of either ±30° or 85±20°. For conformations with χ(CS–SC) close to the ±90° value, the Raman spectra of the 8–25 truncated dimers exhibited χ(SS–CC) dihedral angles of 90/180° and 20–30°. In the presence of a lipid mixture, both constructs showed a ν(S–S) band at ~488 cm^{-1}, corresponding to a χ(CS–SC) dihedral angle of ±10°. Polarized infrared spectroscopy was also used to determine the orientation of the helix and β-sheet portion of both synthetic peptides. These calculations indicated that the helix was oriented primarily in the plane of the surface, at an angle of ~60–70° to the surface normal, while the β structure had ~40° tilt. This orientation direction did not change in the presence of a lipid mixture or with temperature. These observations suggest that: (i) the conformational flexibility of the disulfide linkage is dependent on the amino acid residues that flank the cysteine disulfide bond, and (ii) in both constructs, the presence of a lipid matrix locks the disulfide bond into a preferred conformation.

Keywords: dsp-b_{1-25}; dsp-b_{8-25}; Surfactant protein (sp)-b; Attenuated total reflectance IR spectroscopy; Raman spectroscopy; Lung surfactant; Synthetic peptide

1. Introduction

Mammalian pulmonary surfactant is a highly specialized substance that contains approximately 85% phospholipid, 7–10% protein, and 4–8% neutral lipid [1,2]. Lung surfactant contains four apoproteins, including two small hydrophobic proteins that are known to enhance the adsorption and dynamic film behavior of phospholipids [1–4]. The lack of surfactant in the under-developed lungs of premature infants is the root cause of Respiratory Distress Syndrome (RDS) [5], while disruption of surfactant activity is linked to the pathophysiology of clinical lung damage seen in Acute Respiratory Distress Syndrome (ARDS) [6–8].

One of the most important components of pulmonary surfactant is the small, hydrophobic, lipid-associated protein SP-B [9]. Endogenous SP-B is critical for normal mammalian survival since hereditary SP-B deficiency is lethal in humans [10,11] and gene knock-outs for this protein are fatal in mice [12,13]. The active form of SP-B is a 79-amino acid fragment (8.7 kDa) [14,15]. *In vivo*, the protein exists as a disulfide-linked homodimer of the 79-residue monomers, i.e. $SP\text{-}B_2$ [16].

Abbreviations: ARDS, acute respiratory distress syndrome; ATR, attenuated total reflectance; A/W, air–water; DPPC, 1,2-dipalmitoyl-*sn*-glycero-3-phosphocholine; DOPG, 1,2-dioleoyl-*sn*-glycero-3-[phosphor-*rac*-(1-glycerol)] (sodium salt); HMP, 4-hydroxymethylphenoxyacetyl-4′-methylbenzyhydrylamine resin; RDS, respiratory distress syndrome; SP-B, pulmonary surfactant protein B; SP-B_{1-25}, synthetic peptide containing the first 25 amino acids of the N-terminal sequence of SP-B; SP-B_{8-25}, synthetic peptide containing amino acids 8–25 of the N-terminal sequence of SP-B; TFA, trifluoroacetic acid; TFE, trifluoroethanol

* Corresponding author. Tel.: +1 706 542 1950; fax: +1 706 542 9454.
E-mail address: dluhy@chem.uga.edu (R.A. Dluhy).

0005-2736/$ - see front matter © 2007 Elsevier B.V. All rights reserved.
doi:10.1016/j.bbamem.2007.01.020

Although the detailed structure of native SP-B is unknown, through structural homology each monomer is postulated to contain multiple amphipathic helices [17,18]. Lately, it has also been proposed that an inter-subunit ion pair/salt bridge forms between the Glu51 residue of one SP-B homodimer and the Arg52 charged residue on a separate SP-B homodimer, thereby creating a "dimer of SP-B dimers", i.e. SP-B_2:SP-B_2 [19,20]. It is believed that this dimer-of-dimers is related to a functional role for SP-B in the cross-linking of lipid membranes.

While SP-B is vital for normal respiratory function, less is known about its specific biochemical mode of action. SP-B is a member of the saposin superfamily of proteins that includes saposin B, saposin C, granulysin and NK-lysin [16,17,21]. This family of proteins is characterized by the presence of multiple amphipathic helical domains with a common backbone connectivity stabilized by disulfide linkages [21]. Six conserved cysteine residues in these proteins form three intramolecular disulfide bonds that define an amphipathic helix hairpin structure known as the "saposin fold" that is estimated to have been conserved for 300 million years [22]. This combination of structural features allow members of this class of proteins to interact with lipids and perform diverse functions [23,24].

The details of the molecular interaction of native SP-B with phospholipids are not yet completely understood. One approach to elucidating the contributions to activity of the different structural regions of SP-B involves the study of synthetic peptide fragments such as SP-B_{1-25}, which incorporates the 25 amino acids in the important N-terminal region of the native protein. The SP-B_{1-25} monomer peptide has been the subject of recent structural and biophysical studies [25–33]. Unfortunately, the monomeric SP-B_{1-25} construct lacks the physiologically important disulfide linkage found in native SP-B. The homodimer of SP-B_{1-25} with a disulfide linkage at Cys 8 (dSP-B_{1-25}) is the simplest peptide construct of SP-B that incorporates a covalent disulfide bond. The dSP-B_{1-25} homodimer has been shown to have *in vitro* and *in vivo* activity that is more effective than that of the SP-B_{1-25} peptide monomer, suggesting that the disulfide linkage impairs tertiary structural and functional properties not associated with the monomeric sequence *per se* [34–37].

In this report we use Raman spectroscopy to study the conformation of the disulfide linkage of Cys 8 in the dSP-B_{1-25} homodimer and compare it with the truncated sequence of the disulfide-linked, dimeric 8–25 fragment (dSP-B_{8-25}). The Raman spectra of these two constructs demonstrates that the presence of the flanking hexapeptide in the full length SP-B_{1-25} sequence induces a highly strained nature in the disulfide conformation that is relaxed in the truncated sequence. Our results suggest that this disulfide conformational flexibility may be an important element in identification of critical structural determinants for optimal activity of peptides in surfactant lipids.

2. Experimental methods

2.1. Synthetic materials

The synthetic phospholipid 1,2-dipalmitoyl-*sn*-glycero-3-phosphocholine (DPPC) as well as 1,2-dioleoyl-*sn*-glycero-3-[phosphor-*rac*-(1-glycerol)] (sodium salt) (DOPG) were purchased from Avanti Polar Lipids (Alabaster, AL). These lipids were specified as >99% pure, and were used as supplied. ACS grade NaCl and high-performance liquid chromatography (HPLC) grade methanol and chloroform were obtained from J.T. Baker (Phillipsburg, NJ). Ultrapure H_2O used in all cleaning procedures was obtained from a Barnstead (Dubuque, IA) ROpure/Nanopure reverse osmosis/deionization system, and had a nominal resistivity of 18.3 MΩ cm.

2.2. Peptide synthesis and purification

SP-B_{1-25} (NH_2-FPIPLPYCWLCRALIKRIQAMIPKG-COOH) and SP-B_{8-25} (NH_2-CWLCRALIKRIQAMIPKG-COOH) were made by solid-phase peptide synthesis employing O-fluorenylmethyl-oxycarbonyl (Fmoc) chemistry. Fmoc amino acids and coupling agents were from AnaSpec (San Jose, CA). Solvents and other reagents used for peptide synthesis and purification were HPLC grade or better (Fisher Scientific, Tustin, CA; Aldrich Chemical, Milwaukee, WI). The peptide was synthesized on a 0.25-mmol scale with an ABI 431A peptide synthesizer configured for FastMoc™ double coupling cycles [38] utilizing a pre-derivatized N-α-Fmoc-glycine HMP resin (AnaSpec, San Jose, CA). Deprotection and cleavage of the peptide from the resin was carried out using TFA/thioanisol/EDT/phenol/water (10:0.5:0.25:0.5:0.5 by vol.) for 2 h followed by precipitation cold with t-butyl ether. The crude product was then purified by preparative reverse phase HPLC with a Vydac C-18 column and a water/acetonitrile linear gradient with 0.1% trifluoroacetic acid as described previously [25]. The molecular weight of the monomeric peptides was determined by fast atom bombardment and/or MALDI-TOF mass spectrometry, and purity of >95% was confirmed by analytical HPLC and capillary electrophoresis. The reduced material was then oxidized in 10 mM ammonium acetate buffer, pH 7.5 with trifluoroethanol (6:4, v:v) at a concentration of 1.0 mg peptide/mL for 48 h with stirring at 25 °C to form disulfide linked dimers. The covalently linked constructs were separated from any residual monomeric material by reverse phase HPLC as described for the reduced material and the mass confirmed by electrospray mass spectrometry. The homodimeric peptides were then twice freeze dried from 10 mM HCl solution to remove any residual acetate counter ions prior to Raman and FTIR analysis.

2.3. Preparation of lipid–peptide mixtures

Stock phospholipid solutions of DPPC and DOPG (1 mg/mL) were prepared in 3:1 $CHCl_3$:MeOH. For 4:1 DPPC:DOPG+10% dSP-B_{1-25}/$_{8-25}$, phospholipid–protein mixtures, the required volume of dSP-B_{1-25} or dSP-B_{8-25} in 1:1 $CHCl_3$:MeOH was evaporated with N_2 for ~30 min to ensure complete solvent evaporation. The dried protein film was then dissolved in a volume of 2,2,2-trifluoroethanol (TFE). An appropriate volume of a 4:1 (mol:mol) DPPC:DOPG stock phospholipid solution was then added to the protein solution in TFE. The resultant phospholipid–protein solution was again purged with N_2 for ~45 min and left overnight in a vacuum desiccator for complete elimination of solvent. The dried lipid–protein sample was then dissolved in 3:1 $CHCl_3$:MeOH for use in the IR or Raman studies.

2.4. Raman Spectroscopy

Raman spectra were acquired using a fiber-optic-interfaced, confocal near-IR Raman microscope. The near-IR Raman excitation wavelength of 785 nm was generated using a solid-state tunable Ti:Sapphire ring laser (Model 890, Coherent, Inc., Santa Clara, CA) pumped by a Coherent Innova 300 Series Ar^+-ion laser. A wavelength-specific 785 nm holographic band-pass filter (Kaiser Optical Systems, Ann Arbor, MI) was used to filter the laser radiation, to ensure beam quality, and steer the output of the Ti:Sapphire laser onto a graded refractive index (GRIN) lens (SELFOC, NSG, Inc., Somerset, NJ). The GRIN lens was directly coupled to the surface of an integrated single-mode (ϕ ~7 μm) optical fiber. The distal end of the optical fiber connected to a fiber-optic input/output module (HoloLab Series 5000, Kaiser Optical Systems, Ann Arbor, MI) that delivered the excitation radiation to an Olympus BX-60 research light microscope. A 20× (NA 0.40) apochromatic microscope objective was used both for delivery of the excitation wavelength and collection of the 180° backscattered Raman-scattered radiation. The Raman scattered light collected by the microscope was delivered to an *f*/1.8 holographic imaging spectrograph

(HoloSpec *f*/1.8I, Kaiser Optics) using a fiber optic interface. The detector on this spectrograph was a Princeton Instruments liquid-N_2 cooled CCD detector (1024EHRB, 1024×256 pixels) that was back-illuminated and specifically optimized for high QE in the near-IR spectral region (~35% at 1000 nm).

Gold-coated ITO-glass slides were used as substrates for Raman spectroscopy, as they offered better temperature regulation and S/N ratio, than normal glass microscopic slides. These substrates were prepared by vapor deposition of Au onto standard ITO-covered glass slides (Delta Technologies, Ltd., Stillwater, MN) using an Edwards Auto 306 Vacuum Evaporator (Edwards High Vacuum Inc., Norfolk, UK) in the UGA Center for Ultrastructural Research. Prior to Au deposition, an underlying layer of Cr was first vacuum-deposited onto the glass substrate to promote adhesion of the Au to the glass. These glass slides were precut to pieces of approximately 2.5 cm×1 cm and thoroughly cleaned using Hellmanex®II (Helma GmbH and Co KG, Germany) before the deposition of the Cr and Au. A Physitemp (Physitemp Instruments, Inc., Clifton, NJ) TS-4ER thermal microscope stage and a controller were used for temperature regulation of the ITO gold coated slides.

The synthetic SP-B peptides dSP-$B_{1–25}$ and dSP-$B_{8–25}$ were prepared by dissolving the peptides in a 3:1 $CHCl_3$:CH_3OH mixture to make a 1 mg/mL stock solution. Samples were prepared by spreading 150–200 μL of the dimer solution (1 mg/mL) from a 3:1 $CHCl_3$:MeOH solution onto the Au surface of a Au/Cr vapor-deposited, ITO-coated glass slide. Solvent evaporation led to the formation of dry films which were then spectroscopically analyzed.

2.5. Attenuated Total Reflectance IR Studies

Polarized attenuated total reflection infrared spectra (ATR-IR) were acquired using a Digilab FTS 7000 (Randolph, MA) spectrometer, equipped with a narrow band LN_2-cooled HgCdTe detector (Infrared Associates, Inc., Stuart, FL). The spectra were recorded at various temperatures with 400 co-added scans at 4 cm^{-1} resolution using a triangular apodization function. A 45° Ge crystal (50×10×2 mm) was mounted onto a horizontal ATR accessory (Horizon™, Harrick Scientific Corporation, Ossining, NY) and was temperature regulated using an automatic temperature controller. A KRS-5 wire grid polarizer (Molectron Detector, Portland, OR) was introduced into the optical path prior to the ATR accessory to polarize the incident beam either horizontally or vertically. ATR spectra were acquired using a background spectrum of the Ge crystal for both polarizations at each temperature (30, 40, 50, 60 °C) before spreading the samples.

Protein films were prepared by spreading 150–200 μL of the 1 mg/mL dSP-$B_{1–25}$ or dSP-$B_{8–25}$ solutions in 3:1 $CHCl_3$:CH_3OH onto the Ge crystal and the dry films formed after solvent evaporation, were then analyzed. Hydrated lipid–protein samples were prepared by dispersion of the phospholipid–protein mixture in water after evaporation of the solvents ($CHCl_3$:MeOH) from 4:1 DPPC:DOPG+10% dSP-$B_{1–25}$/$_{8–25}$. Repeated vortexing during heating (up to 60 °C) and cooling (to 0°) cycles resulted in a milky white suspension, which was used in the spectroscopic analysis.

2.6. Orientation Calculations

The orientation of the α-helices and the β-sheets with respect to the film (crystal) normal were calculated from the experimental dichroic ratio values (R^{ATR}) and the electric field amplitudes (E_x,E_z and E_y) using Harrick's 'two phase' approximation [39,40]. The refractive indices of the three phases used were 4, 1.4 and 1 for Ge crystal, sample film and air, respectively. For the α-helices, the dichroic ratios were obtained by ratioing the amide I band intensities for *p*- and *s*-polarizations of the incident IR beam [41,42]. Since the helical structures posses an axial symmetry, a uniaxial distribution about the surface normal was assumed and the order parameter, $f(\theta)$, was expressed by the second Legendre polynomial [43]. The mean angle, θ (angle between the helices and the surface normal), was calculated for a range of angles between 24° and 38° at 2° increment (i.e., at 24°, 26°, 28°, 30°, 32°, 34°, 36° and 38°) corresponding to the angle between the transition moment and the helix axis, which are typical for most proteins reported in the literature [44, 45]. The orientation angle, θ, is the average for the ensemble and not the individual values.

The transition moments of β-sheets lack the axial symmetry of the α-helices; therefore two order parameters were required to define their orientation. These angular distributions were obtained using the dichroic ratios from both the amide I and the amide II bands. The three angles defining β-sheet orientation, i.e. α (the angle of the β-sheets relative to the membrane normal), β (the angle by which the β-strand axes are tilted within the sheets) and γ (the angle of the β-strands relative to the membrane normal), were calculated in accordance with previously published methods [46].

To ascertain the orientation of the dimers in the lipid matrix, the acyl chain tilts of the phospholipids were also calculated relative to the surface normal, utilizing the antisymmetric and symmetric CH_2 vibrations at 2918 cm^{-1} and 2850 cm^{-1} [47,48].

An average of the ensemble was assumed during all the orientation calculations.

2.7. Methods for molecular graphics

The molecular graphic images for dSP-$B_{8–25}$ and dSP-$B_{1–25}$ in Fig. 6 were templated from the structure of monomeric SP-$B_{1–25}$ using Ref. [26] and PDB 1DFW by mutating Cysteine 11 to Alanine. These mutated conformers were then optimized as a homo-dimers using ZDOCK [49]. Representative homodimers for dSP-$B_{8–25}$ and dSP-$B_{1–25}$ were selected from a 100 conformer set generated by the docking program. Selection criteria was based on the helix axis angles and disulfide dihedrals that corresponded to the experimentally observed valves from the IR and Raman measurements. Peptide backbone dihedrals were determined by analysis of the ZDOCK coordinate sets for the docked peptides using the Hyperchem 7.5 secondary structure assignment utility. The helical axis angles were determined using MolMol [50] and the final graphics illustrations were prepared using Pymol [51].

3. Results

3.1. Raman spectroscopy of dSP-$B_{1–25}$

Fig. 1A illustrates the Raman spectra of the dSP-$B_{1–25}$ peptide deposited from organic solution as a thin film on a Au-coated ITO glass slide. Major Raman-active bands apparent in the spectrum are the amide I (~1656 cm^{-1}), CH_2 and CH_3 bending (~1449 cm^{-1}), amide III (~1300–1200 cm^{-1}), C–S (~708 cm^{-1}), and S–S (~486 cm^{-1}) vibrational modes. The peptide secondary structure of dSP-$B_{1–25}$ can be determined using the Raman amide I and the amide III bands. The Raman spectrum of dSP-$B_{1–25}$ reflects a dominant α-helical content, as seen by the band at 1656 cm^{-1}. This was also supported by a 1260 cm^{-1} band in the amide II region and the 935 cm^{-1} skeletal C–C stretching band in the Raman spectra, both of which are characteristic of α-helices [52]. In the amide III region, a band appears at ~1248 cm^{-1}, indicating the presence of small amounts of β-structure in the dimer. The strong 1449 cm^{-1} peak is due to the CH_2 and the CH_3 bending modes, while the C–N stretching vibration is seen as a weak band at ~1100 cm^{-1}. These bands remained invariant with temperature over the range 20 to 70 °C (Table 1).

The conformation of the disulfide bond in dSP-$B_{1–25}$ was analyzed using the S–S stretching vibrations in the 400–600 cm^{-1} region (Fig. 2A). As seen in this figure, the disulfide region for the 1–25 homodimers was marked by a single major peak at 486 cm^{-1} along with minor shoulders at 493, 501 and 520 cm^{-1}. The assignments of these bands are made based on literature precedents that correlate the observed ν(S–S) wavenumber values not only with the χ(CS–SC) dihedral angles but also with the adjacent χ(SS–CC) dihedral angles [53,54], and are presented in Table 2. A more detailed explanation of the conformational assignments of S–S dihedral

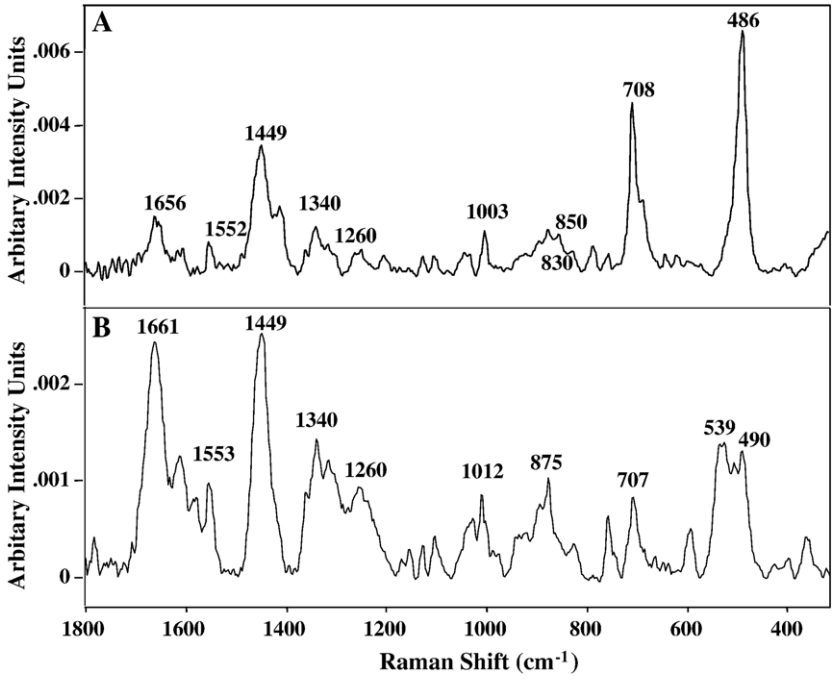

Fig. 1. Raman spectra between 1800 and 300 cm^{-1} in peptide thin films. (A) dSP-B_{1-25}; (B) dSP-B_{8-25}.

angles based on their Raman spectra is presented in Discussion (*vida infra*).

The major ν(S–S) peak in the Raman spectrum of dSP-B_{1-25}, at 486 cm^{-1} (Fig. 2A), is indicative of a highly strained disulfide with a χ(CS–SC) dihedral angle of ±10° [53]. Similarly, the shoulders at 493 cm^{-1} and 501 cm^{-1} were attributed to a strained S–S bond due to a CS–SC dihedral angle in the range of about ±30° and ±60°, respectively. While the Raman spectra of dSP-B_{1-25} provides evidence for the presence of a highly strained disulfide bonds, current theory fails to provide information about the S–S–Cβ′–Cα′ dihedral angle, i.e. χ(SS–CC), for these strained disulfides when χ(CS–SC) varies away from the equilibrium value of ±90°. Therefore, no values for χ(SS–CC) are tabulated for the 486, 493 or 501 cm^{-1} bands (Table 2).

For χ(CS–SC) dihedral angles close to the low energy equilibrium position, i.e. ±90°, is predicted to have ν(S–S) peak above 510 cm^{-1}. However, the actual observed position depends upon the adjacent χ(SS–CC) dihedral conformations. Accordingly, the broad shoulder in the spectrum of dSP-B_{1-25} at ~520 cm^{-1} (Fig. 2A) indicates a χ(CS–SC) value of ±90° and a range of χ(SS–CC) conformations, potentially including those with a S–S–Cβ′–Cα′ dihedral angle of 20–30° (A conformer), 90° (B conformer) or 180° (T conformer), when χ(CS–SC) ~±90° (Table 2) [53,54]. Unfortunately, it is difficult to fully differentiate the dihedral angles in these conformers from the Raman data alone.

Raman spectroscopy of dSP-B_{1-25}, co-solubilized in a lipid matrix of 4:1 DPPC:DOPG, reveals a similar disulfide spectral signature as that of the pure peptide (Fig. 2B). This lipid mixture approximates the neutral/anionic lipid composition found in pulmonary surfactant and has previously been used in biophysical studies of SP-B [32,33].

Table 1
Dichroic ratios ((A_p/A_s)) corresponding to the CH_2 antisymmetric (asym) and symmetric (sym) stretches of 4:1 DPPC:DOPG mixture in the presence and absence of dSP-B_{1-25} and dSP-B_{8-25}, α-helix (of dSP-B_{1-25} and dSP-B_{8-25}) and the β-sheets (of dSP-B_{1-25}) in the presence and absence of 4:1 DPPC:DOPG lipid matrix at 30 °C

Samples	CH_2 (asym) (A_p/A_s)	CH_2 (sym) (A_p/A_s)	Amide I (α-helix) (A_p/A_s)	Amide I (β-sheet) (A_p/A_s)	Amide II (β-sheet) (A_p/A_s)
4:1 DPPC:DOPG	1.407	1.354	–	–	–
dSP-B_{1-25}	–	–	1.69	1.80	1.85
10 wt.% dSP-B_{1-25} in 4:1 DPPC:DOPG	1.328	1.279	1.89	1.95	1.85
10 wt.% dSP-B_{1-25} in 4:1 DPPC:DOPG (hydrated films)	1.132	1.079	1.74	1.81	1.73
dSP-B_{8-25}	–	–	1.72	–	–
10 wt.% dSP-B_{8-25} in 4:1 DPPC:DOPG	1.2432	1.1774	1.48	–	–
10 wt.% dSP-B_{8-25} in 4:1 DPPC:DOPG (hydrated films)	1.6568	1.5971	1.87	–	–

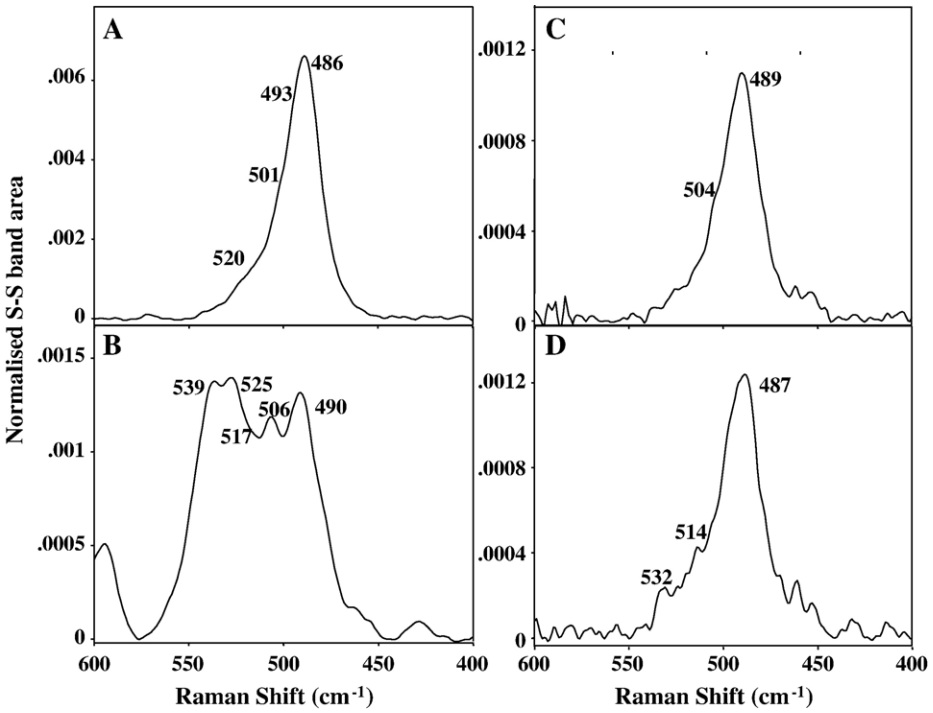

Fig. 2. Raman spectra of the ν(S–S) stretching vibration region between 600 and 400 cm^{-1} in peptide and lipid–peptide thin films at 20 °C. (A) dSP-B_{1-25}; (B) dSP-B_{8-25}; (C) 4:1 DPPC:DOPG+10 wt.% dSP-B_{1-25}; (D) 4:1 DPPC:DOPG+10 wt.% dSP-B_{8-25}.

The strong peak at ~489 cm^{-1} indicates that the highly strained χ(CS–SC) dihedral angle of ±10° is conserved even in the presence of lipids. The only other conformation present is indicated by a small shoulder at 504 cm^{-1}, corresponding to a dihedral angle χ(CS–SC) of ±60°. The dihedral conformation assignments based on the Raman spectra of the 4:1 DPPC:DOPG+10% dSP-B_{1-25} sample are also presented in Table 2.

Table 2
Dihedral angles corresponding to the observed Raman bands in the S–S region of dSP-B_{1-25}, dSP-B_{8-25}, 10 wt.% dSP-B_{1-25} in 4:1 DPPC;DOPG and 10 wt.% dSP-B_{8-25} in 4:1 DPPC:DOPG

	ν(S–S), cm^{-1}	χ(SS–CC), °	χ(CS–SC), °
dSP-B_{1-25}	486	–	±10
	493	–	±30
	501	–	±60
	520	50–180 (B/T); 50–180 (B/T)	±90
dSP-B_{8-25}	490	–	±30
	506	–	±60
	517	50–180 (B/T); 50–180 (B/T)	±90
	525	0–50 (A); 50–180 (B/T)	±90
	539	0–50 (A); 0–50 (A)	±90
10 wt.% dSP-B_{1-25} in 4:1 DPPC:DOPG	489	–	±10
	504	–	±60
10 wt.% dSP-B_{8-25} in 4:1 DPPC:DOPG	487	–	±10
	514	50–180 (B/T); 50–180 (B/T)	±90
	532	0–50 (A); 0–50 (A)	±90

Assignments based on correlations in the S–S Raman spectrum of model compounds [53,54]. χ(SS–CC) values: A: 0–50°, B: 90°, T: 180°.

Temperature dependent studies in the disulfide region of the 1–25 dimer in the presence and absence of the phospholipids matrix (in the range 20–70 °C), revealed a very stable conformation of the disulfide bonds, which remained invariant to the presence of lipids and temperature perturbations (data not shown).

Similar to the disulfide region, the C–S stretching region also provides information concerning protein conformation. The strong band at 708 cm^{-1} and the less intense bands in the 664–690 cm^{-1} range in the spectrum of dSP-B_{1-25} (Fig. 1A) may be attributed to the C–S stretching vibrations from the N–C–C–S–S (*trans* for N and S–S) and the H–C–C–S–S (*trans* for H and S–S) units, respectively [55,56]. The weak shoulder observed at 722 cm^{-1} may be attributed to the C–S stretching vibrations for the *trans* form of the methionine residue.

The intensity ratio of the 850 and 830 cm^{-1} tyrosine doublet (I_{850}/I_{830}) has been used to identify structure in the phenolic hydroxyl group [57]. This doublet arises from Fermi resonance between the ring-breathing vibration and the overtone of an out-of-plane ring-bending vibration of the para-substituted benzene. For dSP-B_{1-25}, the intensity ratio of this doublet varied little with temperature but had a value ≥1. A higher intensity of the 850 cm^{-1} band has been indicative of the tyrosine residue being exposed to a polar environment, where the phenolic hydroxyl group acts as acceptors and donors for moderate H-bonds or in a hydrophobic environment [57,58]. Other tyrosine bands evident in the spectrum of dSP-B_{1-25} are the C–C ring twist at ~643 cm^{-1} and the 1605 cm^{-1} band, which may be due to the ring vibrations in phenylalanine or tyrosine.

The 1361 cm^{-1} band of tryptophan has also been reported as a sensitive indicator of its environment [59–62]. Previous studies have shown that the 1361 cm^{-1} band of the indole ring in tryptophan appears as a sharp feature if the indole ring is buried and broadens with decreasing sharpness, as it becomes exposed to a polar environment. The 1361 cm^{-1} Trp band appears as a relatively sharp band at 20 and 30 °C but gradually broadens with increasing temperature (Fig. 3A). Gordon et al. [25] observed that although the Trp 9 of monomeric SP-$B_{1–25}$ inserts into hydrophobic lipid domains when the peptide is dispersed with zwitterionic/anionic lipids, the residue nonetheless remains solvent accessible. The current data also support the solvent-accessible nature of the Trp residue in oriented thin films of the dSP-$B_{1–25}$ homodimer. The bands in the Raman spectra at ~571, 758, 875, 1553 and 1585 cm^{-1} may also be assigned to the indole-ring vibrations in the Trp residue [63].

Unlike the tyrosine and the tryptophan residues the ring breathing mode of the phenylalanine at 1003 cm^{-1} is not conformation sensitive. This band may also have contributions from the C–C stretch from the lysine residue. The other ring vibrations of the Phe residue are the strong bands at 1033 and 1205 cm^{-1} and the weak bands at 617, 1587 and 1605 cm^{-1}. The bands at 620 cm^{-1} and 1033 cm^{-1} may also be assigned to the phenylalanine residue [64].

3.2. Raman spectroscopy of dSP-$B_{8–25}$

The Raman spectrum of a thin film of the dSP-$B_{8–25}$ homodimer construct is presented in Fig. 1B. This construct was prepared without the leading N-terminal heptapeptide sequence of dSP-$B_{1–25}$, therefore, the covalent disulfide bond between the two monomer units occur at the N-terminal Cys residue. The amide I and amide III bands in the Raman spectrum of the 8–25 dimer appear at ~1661 cm^{-1} and ~1254 cm^{-1} respectively (Fig. 1B). The strong 1661 cm^{-1} peak together with the 1260 and 933 cm^{-1} Raman bands support a helical structure for this peptide, similar to the 1–25 homodimers (Fig. 1A). Again, similar to dSP-$B_{1–25}$, the broad shoulder at ~1234 cm^{-1} indicate the presence of a small amount of random coil or β-structures. The Raman spectra of the 8–25 dimer also show strong bands due to the CH_2 and CH_3 bending modes at 1449 cm^{-1} and weak C–N stretching bands near 1100 cm^{-1}, all of which remain unchanged with temperature (data not shown). A comparison of the spectra for dSP-$B_{1–25}$ and dSP-$B_{8–25}$ in Fig. 1 shows that the helical structure of the dimers is not significantly influenced by the N-terminal heptapeptide segment.

While the overall helix secondary structure appears similar for the two constructs, considerable differences can be observed in the disulfide region of the two dimers (Figs. 2A and C). As discussed above, dSP-$B_{1–25}$ exhibits a single major S–S band at

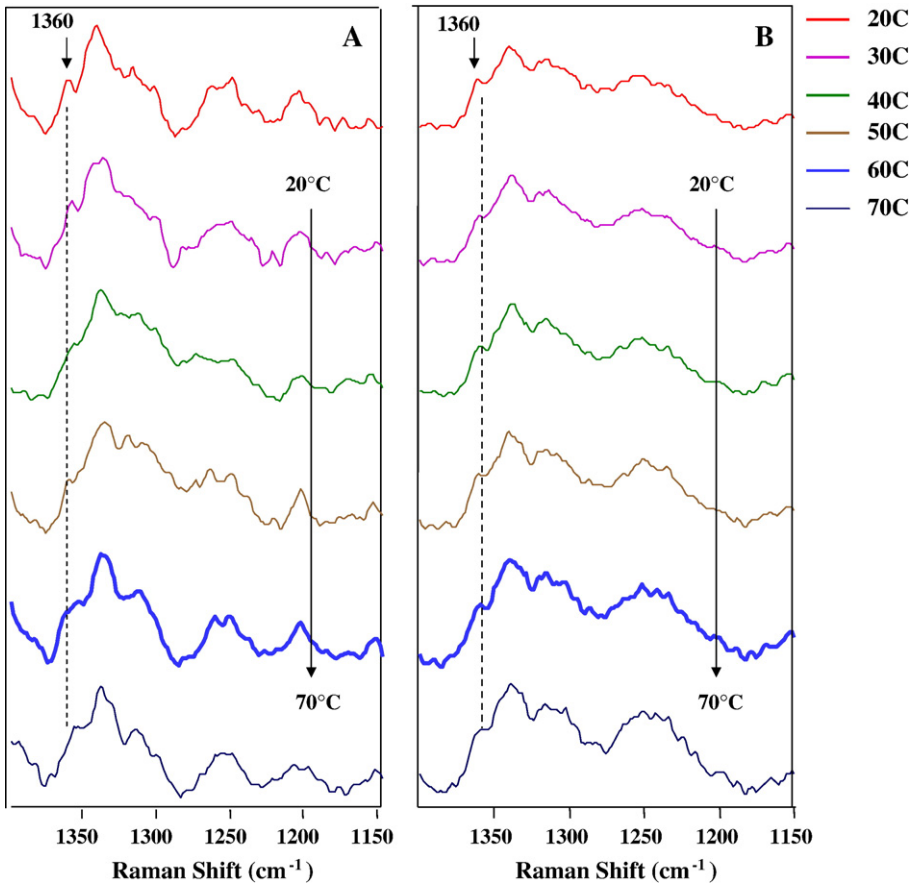

Fig. 3. Raman spectra of the tryptophane spectral region between ~1400 and 1150 cm^{-1} in peptide thin films acquired as a function of temperature between 20 and 70 °C. (A) dSP-$B_{1–25}$; (B) dSP-$B_{8–25}$.

486 cm^{-1} (Fig. 2A), representing a highly strained disulfide geometry. For dSP-$B_{8–25}$, however, a multicomponent spectral contour is seen in the range 550–470 cm^{-1} (Fig. 2C). The major bands in the S–S spectrum of dSP-$B_{8–25}$ at 490 cm^{-1}, 506 cm^{-1}, 525 cm^{-1} and 539 cm^{-1}, can be interpreted in line with the theory described in more detail in Discussion below [53,54]. Analogously to the situation of the 1–25 homodimers, the prominent 490 cm^{-1} and 506 cm^{-1} bands in the S–S spectrum of dSP-$B_{8–25}$ can be explained by the presence of strained disulfide conformations, in these cases with χ(CS–SC) dihedral angle in the range of ±30° and ±60°, respectively. For dSP-$B_{8–25}$, however, three additional bands (517, 525 and 539 cm^{-1}) with significant intensity are present in the spectrum above 510 cm^{-1}. The wavenumber positions of these bands although correspond to a similar χ(CS–SC) dihedral angle close to its minimum energy conformation of ±90°, are distinguished by the χ(SS–CC) dihedral conformations of ([B or T], [B or T]), (A, [B or T]), and (A, A). The A, B and T conformations are defined by χ(SS–CC) values of ~20–30°, 90° and 180° [53,54]. The assignments for the Raman spectra of dSP-$B_{8–25}$ are presented in Table 2.

Unlike in case of dSP-$B_{1–25}$, the disulfide region for the 8–25 dimer, interestingly, showed major conformational changes upon incorporation in the phospholipid matrix. The disulfide region in the Raman spectrum of a 4:1 DPPC:DOPG+10% dSP-$B_{8–25}$ is shown in Fig. 2D. In contrast to a multi-band contour with heterogeneous disulfide conformations for the pure 8–25 construct, the 8–25 dimer was dominated by a single band at 487 cm^{-1}, when co-solubilized in a phospholipid matrix. This wavenumber value corresponds to a highly strained χ(CS–SC) dihedral angle of ±10° (similar to that of dSP-$B_{1–25}$, both in the presence and absence of lipids) (Fig. 2). Minor peaks were observed at 514 and 532 cm^{-1} (Fig. 2D). These bands indicate the presence of a small amount low energy χ(CS–SC) dihedral conformation of ±90°, along with S–S–Cβ′–Cα′ conformations of 50° (A conformer), 90° (B conformer) or 180° (T conformer) [53,54]. The dihedral angle conformation assignments based on the Raman spectra of the 4:1 DPPC:DOPG + 10% dSP-$B_{8–25}$ sample are presented in Table 2.

However, temperature variation studies (20–70 °C) of the 8–25 dimer (both alone and in a lipid matrix), portrayed the invariant nature of the spectral features with temperature, similar to its 1–25 counterpart, indicating stable conformations.

Unlike the S–S region, the C–S region is similar in both the dimers. Fig. 1B shows that the C–S stretching region for dSP-$B_{8–25}$ is marked by a strong band at ~707 cm^{-1}, due to the *trans* form of the N–C–C–S–S unit (*trans* with respect to the N and the SS unit) [55,56,65], and a weak band at ~663 cm^{-1} from the H–C–C–S–S unit (trans with respect to the H and the SS unit). The 722 cm^{-1} band corresponding to the *trans* form of the methionine residue [56,64–66] is also preserved in dSP-$B_{8–25}$.

The tryptophan doublet originating from Fermi resonance between the N_1C_8 (W7) stretching mode and the combination of the out-of-plane deformation modes [67] appear at 1340 and

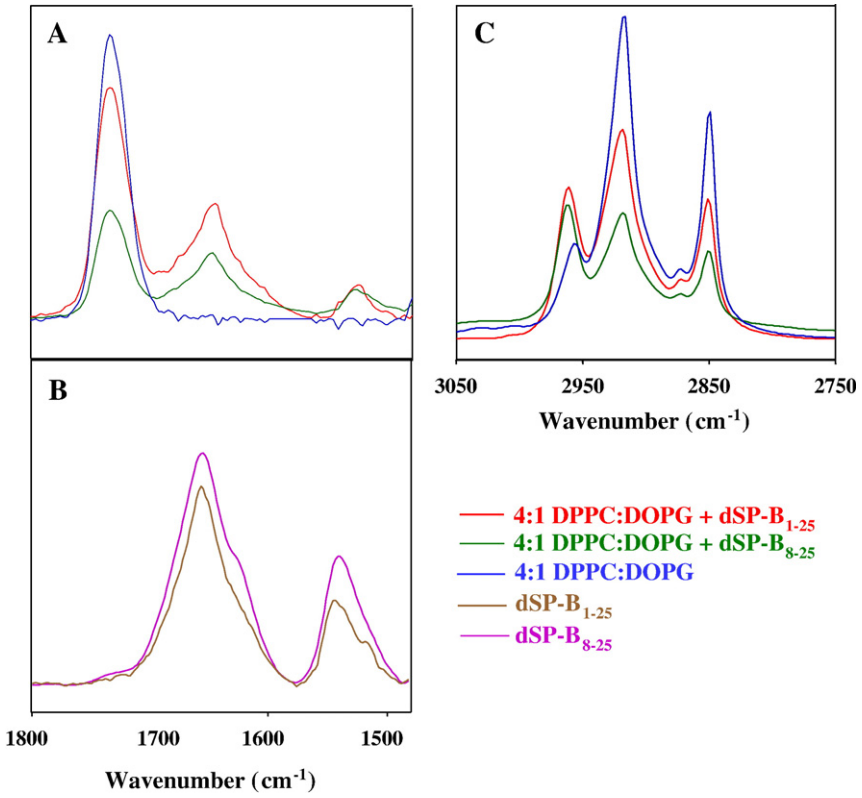

Fig. 4. Polarized ATR-IR spectra of the amide I, amide II and the C–H regions in lipid, peptide and lipid–peptide thin films at 30 °C. (A) 1800–1500 cm^{-1} spectral range for 4:1 DPPC:DOPG, 4:1 DPPC:DOPG+10 wt.% dSP-$B_{1–25}$ and 4:1 DPPC:DOPG+10 wt.% dSP-$B_{8–25}$; (B) 1800–1500 cm^{-1} spectral range for dSP-$B_{1–25}$ and dSP-$B_{8–25}$; (C) 3050–2750 cm^{-1} spectral range for 4:1 DPPC:DOPG, 4:1 DPPC:DOPG+10 wt.% dSP-$B_{1–25}$ and 4:1 DPPC:DOPG+10 wt.% dSP-$B_{8–25}$. All the spectra were acquired with the polarizer parallel to the plane of incidence.

1360 cm^{-1} in dSP-$B_{8–25}$ (Fig. 3B). The broad structure of the 1360 cm^{-1} bands was comparable in both dimers (Figs. 3A and B). The bands in the Raman spectra at ~758, 877, 1554 and 1582 cm^{-1} were attributed to the indole-ring vibrations in the Trp residue [63]. The Arg residues at 12 and 17 probably also have contributions to the 1582 cm^{-1} band.

3.3. Polarized ATR spectroscopy—conformation and orientation of the helix

We examined the peptide conformation and orientation in thin films of the two SP-B dimers using temperature-dependent polarized ATR-IR spectroscopy. The molecular order parameters were calculated from the dichroic ratios using the amide I region for (α-helices), both the amide I and II regions (for β-sheets) and the antisymmetric ($\nu_a(CH_2)$) and symmetric ($\nu_s(CH_2)$) vibrations of the CH_2 bands for the acyl chain tilts in the phospholipid films. Table 1 summarizes the dichroic ratios for the pure phospholipid matrix and the phospholipids in the presence and absence of the dimers at 30 °C. Since, temperature variations did not yield significant changes, data are not shown.

Fig. 4 shows the amide I and amide II regions in the *p*-polarized ATR spectra of thin films of 4:1 DPPC:DOPG, 4:1 DPPC:DOPG+10 wt.% dSP-$B_{1–25}$ and 4:1 DPPC:DOPG+10 wt.% dSP-$B_{8–25}$ (Fig. 4A). Figs. 4B and C display the amide I and amide II regions of the pure peptide films and the C–H region of the phospholipids film in the presence and absence of the 1–25 and the 8–25 dimer, respectively. The prominent peak at ~1655 cm^{-1} suggests a predominantly α-helical conformation (with small amounts of β-sheet structures) for the pure peptide films (Fig. 4B), that is retained even in the phospholipids matrix (Fig. 4A) [25,26,33]. The major 1740 cm^{-1} band in Fig. 4A, is the carbonyl vibration from the C═O group in the phospholipids. No significant polarization-dependent or temperature-dependent spectral changes occurred when using *s*-polarization and on increasing the temperature from 30 to 60 °C (data not shown), suggesting stable conformations.

Assuming a uniaxial model, the orientation distribution of the helix axis with the surface normal (θ) varied from 60° to 70° for the reported range of transition moment tilt (24°–38°) [44,45] for both the 1–25 and 8–25 SP-B dimers. Incorporation of the dimers into lipid–peptide mixtures did not change the orientation of the helix. While different orientation angles of the helix axis has been reported in the literature for the SP-$B_{1–25}$ [25,30,68], almost all agree to a tilted model of the helix, as in the present study.

β-sheet orientation calculations for dSP-$B_{1–25}$, revealed β-strands, tilted at angles of 44° within the sheets which possessed angular distributions of roughly 55°–57° with respect to the membrane normal. The angle by which the planes of the sheets were tilted to the membrane normal varied between 37° and 41°. These calculations were based on a non-axial symmetry model, which used the dichroic ratios from both the amide I and amide II regions to completely define the order parameters of the β-sheets [46].

The effect of these dimers on the phospholipids film was also ascertained by comparing the tilt of the hydrocarbon chains in the presence and absence of the dimers. The asymmetric and the symmetric vibrations of the methylene groups appear at 2918 cm^{-1} ($\nu_a(CH_2)$) and 2850 cm^{-1} (($\nu_s(CH_2)$), respectively, indicating an all-*trans* configuration (Fig. 4C). Assuming an infinitely narrow orientation distribution, the acyl chain tilt angles were found to be approximately 34° (for the ($\nu_s(CH_2)$) band) in pure lipid films. With the incorporation of the dimers, the acyl chain tilts were ~31° for dSP-$B_{1–25}$ and ~27° (using ($\nu_s(CH_2)$) for the 8–25 dimer. However, upon hydration, the hydrocarbon chains tilted more towards the surface normal for dSP-$B_{1–25}$ (to ~22°), while it tilted slightly away from the normal for dSP-$B_{8–25}$ (to ~42°), using symmetric CH_2 stretches, respectively. Using the $\nu_a(CH_2)$ band, varied the tilt angles by approximately ±2°. Similar to the protein secondary structures, the lipid acyl chains too, did not vary appreciably with temperature (data not shown).

One notable feature in the ATR-IR spectra of the lipid–peptide complexes occurred in the phospholipid head group region. Fig. 5 shows the mid-IR spectra between 1800 and 900 for: dSP-$B_{1–25}$; dSP-$B_{8–25}$; 4:1 DPPC:DOPG; 4:1 DPPC:DOPG+10 wt.% dSP-$B_{1–25}$; and 4:1 DPPC:DOPG + 10 wt.% dSP-$B_{8–25}$. The bands centered at ~1250 cm^{-1} and 1080 cm^{-1} are assigned to the antisymmetric and symmetric PO_2^- stretching vibrations of the phosphate group in the phospholipid head group, while the band in the 900–800 region is the single bond P–O stretching vibration [69]. The weak bands in this spectral region for the pure peptide films may be due to some complex ring vibrations. As is evident from the figure, the bands in this region show a marked increase in intensity when the SP-B dimers are incorporated into the lipid mixture. This is suggestive of possible electrostatic interactions between the hydrophilic charged residues of the dimeric peptides and the polar phospholipid head groups. Similar

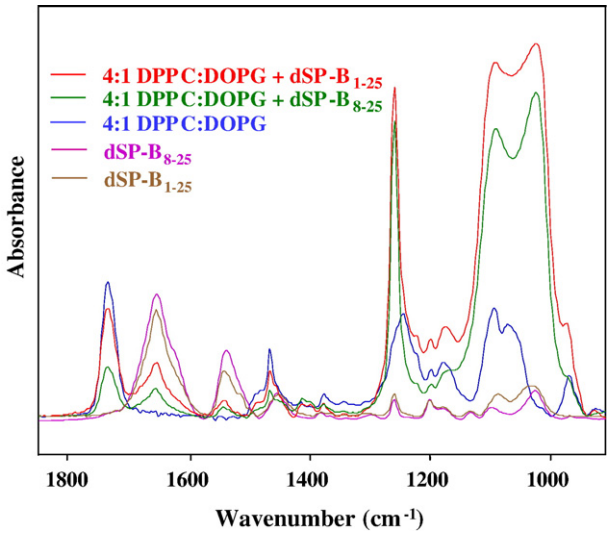

Fig. 5. Polarized ATR-IR spectra of dSP-$B_{1–25}$, dSP-$B_{8–25}$, 4:1 DPPC:DOPG, 4:1 DPPC:DOPG+10 wt.% dSP-$B_{1–25}$, and 4:1 DPPC:DOPG+10 wt.% dSP-$B_{8–25}$ thin films at 30 °C. The spectra were acquired with the polarizer parallel to the plane of incidence.

ordering of phosphocholine/phosphoglycerol bilayers in the presence of SP-B has been previously reported [70,71].

4. Discussion

The hydrophobic surfactant protein B (SP-B) is a functionally essential component of endogeneous lung surfactant, with multiple amphipathic domains that interact with both the hydrophobic and hydrophilic regions of phospholipids [16]. SP-B undergoes post-translational modification to form disulfide bonds [72,73]. *In vivo*, SP-B exists as a homodimer with three intramolecular disulfide bridges (i.e. Cys8–Cys77, Cys11–Cys71 and Cys35–Cys46) and one intermolecular disulfide bond between the cysteine residues at position 48 of each monomeric unit [73,74].

Since, SP-B_{1-25} has been shown to mimic many of the physiological effects of the full-length protein, it has formed the basis for many studies, particularly its dimeric form, which recently has been reported as more efficient than the monomeric counterpart in reducing the surface tension in surface films [34].

In order to gain insight into the functional aspects of the disulfide linkages in SP-B, Raman spectroscopy was used to investigate the disulfide dihedral conformation in the synthetic SP-B dimeric constructs dSP-B_{1-25} and dSP-B_{8-25}. We also employed polarized ATR-IR spectroscopy to study the conformation and orientation of the peptide sequence. These experiments were performed on the pure synthetic dimers alone as well as when they were incorporated into a phospholipid mixture. This is the first report of a detailed study of the conformation of the disulfide bond in SP-B.

The ν(S–S) stretching vibration appears as a highly intense Raman band in the 550–450 cm^{-1} region, making Raman spectroscopy a useful tool for characterization of this bond in proteins [52]. However, interpretation of disulfide conformation based on the Raman ν(S–S) mode is not straightforward, as several competing theories have been described that discuss how to correlate wavenumber with conformation. One model suggests that the wavenumber position of ν(S–S) is dependent upon the torsional angles in the Cα–Cβ–S–S–Cβ′–Cα′ conformation [55,75]. In this case, the ν(S–S) band position appears at 510 cm^{-1} for the lowest energy *gauche–gauche–gauche* (g–g–g) conformation, at 525 cm^{-1} for the higher energy *gauche–gauche–trans* (g–g–t) conformation, and at 540 cm^{-1} for the highest energy *trans–gauche–trans* (g–t–g) conformation. This interpretation implies that the wavenumber position of ν(S–S) vibration is dependent only on the internal rotation about the C–S and C–C bonds in the Cα–Cβ–S–S–Cβ′–Cα′ conformation. However, this theory based on torsional rotation, fails to account for the low wavenumber values (~490 cm^{-1}) we experimentally observe in the S–S spectra of these homodimers.

A different interpretation of Raman disulfide conformation suggests that the ν(S–S) values are dependent upon dihedral angles and that there is no simple correlation of ν(S–S) with torsional rotation of the C–S bonds [53,54,76]. Rather, this theory suggests a linear correlation between ν(S–S) and Cβ–S–S–Cβ′ dihedral angle. Different structural constraints are assumed to influence the S–S bond causing a deviation in the dihedral angle χ about the Cβ–S–S–Cβ′ group from the equilibrium value of ~90° (±30°) to something in the range of 0–60° or 110–180°. The strain in the S–S bond is reflected in the ν(S–S) bands below 510 cm^{-1}.

The dihedral angle based interpretation also suggests, that the wavenumber value for the ν(S–S) vibration containing the Cα–Cβ–S–S–Cβ′–Cα′ molecular group should range from about 540–485 cm^{-1}, with wavenumber dependence not only upon the dihedral angle of the Cβ–S–S–Cβ′ group, but also of the adjacent Cα–Cβ–S–S and S–S–Cβ′–Cα′ groups. Disulfides with S–S–Cβ′–Cα′ dihedral angles of 180° and/or ±90°, will have ν(S–S) values near 510 cm^{-1}. These conformations have been defined as "T" and "B" conformations respectively. Disulfides with S–S–Cβ′–Cα′ dihedral angles near 30° about one or both of their C–S bonds give rise to ν(S–S) vibrations between 540 and 525 cm^{-1}. For example, the ν(S–S) band near 525 cm^{-1} results from a small value of the Cα–Cβ–S–S dihedral angle while the ν(S–S) band near 540 cm^{-1} arises from the presence of a conformation with a value of ~30° for the Cα–Cβ–S–S dihedral angle (defined as "A" conformation) [54]. While most of the observed ν(S–S) vibrations exist between 500 and 540 cm^{-1}, strained disulfide groups with Cβ–S–S–Cβ′ dihedral angles less than ±65° also exist [53], and this is unaccounted for in the previous theory [55,75].

We based our analysis of the Raman disulfide data in dSP-B_{1-25} and dSP-B_{8-25} on the dependence of ν(S–S) on dihedral angles rather than torsional rotation. We believe that this interpretation accounts for the low wavenumber values (~490 cm^{-1}) we experimentally observe in the S–S spectra of these homodimers. Torsional rotation alone cannot account for these data. While the dihedral angle theory better describes our data, it does contain two significant drawbacks: (i) the inability to precisely identify Cβ–S–S–Cβ′ dihedral angles other than ±90°, and (ii) the lack of information about the Cα–Cβ–S–S or S–S–Cβ′–Cα′ dihedral angles when the Cβ–S–S–Cβ′ dihedral angle does not equal ±90°. In these cases, we have indicated the presumed dihedral angles within the ranges prescribed by the theoretical interpretation.

The Raman spectra for the dSP-B_{1-25} dimer show a strong peak at 486 cm^{-1}, with minor peaks at 493, 501 and 520 cm^{-1} (Fig. 2A). Several conclusions are possible from analysis of the disulfide bands in the Raman spectra of dSP-B_{1-25}:

- The 1–25 homodimer possesses a predominantly highly strained, yet stable disulfide conformation with a χ(CS–SC) dihedral angle in the range of ±10°.
- A small percentage of the 1–25 homodimer orients in a more stable, low energy conformation with a χ(CS–SC) dihedral angle of ±90°.
- The disulfide conformation of the 1–25 homodimers is virtually unchanged in the presence of a lipid matrix, maintaining the highly strained, yet stable disulfide conformation with a χ(CS–SC) dihedral angle in the range of ±10°.

Interestingly, the Raman disulfide bands in the spectrum of the 8–25 dimer differed significantly from those of the 1–25 peptides. Of note, is the significant conformational changes of the 8–25 dimer upon incorporation into the 4:1 DPPC:DOPG phospholipid matrix. Instead of the multi-component signature pattern spanning the entire ν(S–S) region, the dSP-B_{8-25} in presence of lipids is dominated by a single major peak at 487 cm^{-1}, similar to that of dSP-B_{1-25} (Fig. 2).

Analysis of the Raman spectra of the disulfide region of dSP-B_{8-25} permits the following conclusions:

- Like the 1–25 construct, the 8–25 homodimers possesses a certain amount of a highly strained, yet stable disulfide conformation with a χ(CS–SC) dihedral angle in the range of ±10°.
- However, unlike the 1–25 construct, majority of the 8–25 homodimers orients in the more stable, low energy conformation with a χ(CS–SC) dihedral angle of ±90°.
- When the χ(CS–SC) dihedral angle is ±90° in the 8–25 dimer, the χ(SS–CC) dihedral angle can take on a range of higher energy, strained conformations.
- The absence of the first seven amino acid residues of the N-terminal in dSP-B_{8-25} results in a more stable, low energy conformation of the χ(CS–SC) dihedral angle. However, this comes at the expense of higher energy conformations in the adjacent χ(SS–CC) dihedral angles.
- Significant changes in the conformation around the disulfide bonds are observed when it is co-solubilized in a lipid matrix. Instead of multiple conformations, the 8–25 dimer assumes a predominantly highly strained disulfide conformation (χ(CS–SC) ~±10°) in the presence of lipids, similar to that of dSP-B_{1-25}.

Temperature-dependent studies were performed by subjecting the peptide and lipid–peptide films to temperature variations in the range of 20°–70 °C. The laser power at the sample stage was approximately 10–15 mW, using the near-IR 785 nm incident beam. The use of the near IR laser beams, reduce the fluorescence interference and the heating effect on the sample at these low laser powers. Both dimers in the presence and absence of phospholipids demonstrated very stable conformations that did not alter with temperature changes (data not shown).

Polarized ATR-IR studies of the peptides revealed a predominantly helical conformation for both the dimers distinguished by a strong band centered at ~1655 cm^{-1}, with minor contributions from β-sheet conformations at ~1630 cm^{-1}. In the present study, although a predominance of the α-helical component was observed for both dimers, the broadness of the amide I band (full width at half-height) is indicative of the presence of various conformations. These results are in agreement with previous secondary structural studies by Gordon et al. [25], of the 1–25 and the 8–25 dimer. The conformation of the peptides, did not change in the presence of a lipid mixture. This was expected as the N-terminal heptapeptide segment of SP-B (SP-B_{1-7}) is comprised of three equally spaced proline residues. The absence of an amide hydrogen for H-bonding and steric hindrance caused by the five-membered ring in Pro, restricts rotation about the Cα–N bond, and therefore, disfavors α-helix formation.

It is interesting to note the enhancement of the spectral intensity in the phospholipid headgroup region (1300–900 cm^{-1}) in the presence of the dimeric peptides (Fig. 5). The bands due to the asymmetric PO_2^- stretch, symmetric PO_2^- stretch and the CO stretch involving the PO single bond stretch, had a marked increase in intensity when compared to the pure lipid or protein films. This may be the direct consequence of the previously suggested lipid–protein interactions between the hydrophilic residues of the protein and the polar headgroups [70,71]. The infrared results may also be possibly correlated to the previous epifluorescence study done in our laboratory [32] with 10% mSP-B_{1-25} in a 4:1 DPPC:DOPG mixture, wherein the peptide was observed to be more strongly associated with the DOPG component of the lipid mixture, resulting in fluorescence micrographs having more DPPC character. The present ATR results are also consistent with the literature precedents of SP-B induced

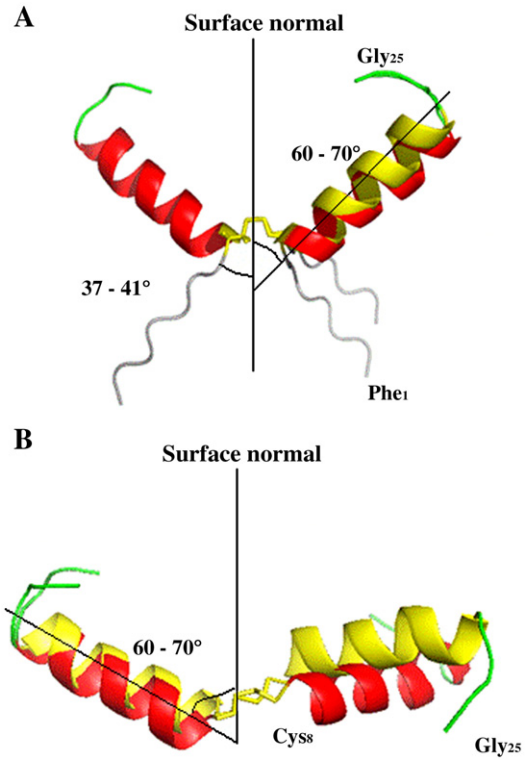

Fig. 6. Molecular graphic illustrations of homodimeric peptides. (A) dSP-B_{1-25}; N-terminal beta sheet elements residues 1–7 and type three turn residues 8–9 in gray, helical secondary structure residues 10 to 21 in red and yellow, and C-terminal beta sheet and random structures residues 22–25 in green; (B) dSP-B_{8-25}; helical segments in red or yellow residues 8–21, beta sheet and random structure residues 22–25. The helical axes of the dimers colored in red and yellow are oriented approximately 60° from the substrate normal. The yellow helix segments represent disulfide linkages with dihedrals −90° while the red colored helixes indicate disulfide connectivities of +90° for dSP-B_{8-25}. The yellow helical segments for dSP-B_{1-25} reflect disulfide connectivities of −10° while the red helical segments are disulfide linkages near +10°. (For interpretation of the references to colour in this figure legend, the reader is referred to the web version of this article.)

increased ordering of phosphocholine/phosphoglycerol bilayers [70,71] and support the interaction of the hydrophilic residues of the SP-B dimers with the phospholipid headgroups, while the hydrophobic residues interact with the acyl side chains.

The orientations of the peptide secondary structures have been summarized in the illustration in Fig. 6. Quantitative conformational analysis of the helix, using polarized ATR spectroscopy revealed a stable and an almost parallel orientation of the helix along the membrane surface, which did not show appreciable changes with temperature variance. These tilt angles are the average values calculated for an ensemble, rather than for the individual molecules. Assuming uniaxial orientation and a transition dipole moment of 24°–38° for the amide I mode, the helix was determined to be oriented at approximately 60–70° from the ATR crystal normal (Fig. 6A). There appears to be small deviations in the reported helix orientations for SP-B_{1-25} peptide in the literature [25,30], although most models assign a value close to 40–50° to the angle between the helix and the surface normal. Wang et al., predicted an almost parallel orientation of the helix along the membrane surface [68]. The small deviations in these reported values may be attributed to the different experimental conditions subjecting the samples. In the present study, the helix orientation was identical for both the 1–25 and 8–25 SP-B dimers (Figs. 6A and B), and did not change with temperature or in the presence of lipids. The large angular value for the helix tilt (60–70°) relative to the surface normal is suggestive of an almost parallel orientation of the helix along the membrane surface. Again, the enhancement of ATR-IR intensity in the 1300–900 cm^{-1} spectral region in a lipid environment (Fig. 5), may be attributed to the interaction of the charged residues of the peptides with the phospholipids headgroups. These results together suggest a model with the dimers lying parallel to the membrane surface rather than being embedded in the lipid bilayer, similar to predictions by Wang et al. [68].

Acknowledgements

The financial support of the U.S. Public Health Service through National Institute of Health (NIH) grants EB001956 (RAD) and HL55534 (FJW and AJW) is gratefully acknowledged.

References

[1] R.H. Notter, Lung Surfactants: Basic Science and Clinical Applications, Marcel Dekker, Inc., New York, 2000.
[2] L.A.J.M. Creuwels, L.M.G. van Golde, H.P. Haagsman, The pulmonary surfactant system: biochemical and clinical aspects, Lung 175 (1997) 1–39.
[3] S. Hawgood, K. Schiffer, Structures and properties of the surfactant-associated proteins, Annu. Rev. Physiol. 53 (1991) 375–394.
[4] J. Johansson, T. Curstedt, B. Robertson, The proteins of the surfactant system, Eur. Respir. J. 7 (1994) 372–391.
[5] M.E. Avery, J. Mead, Surface properties in relation to atelectasis and hyaline memrane disease, Am. J. Dis. Child. 97 (1959) 517–523.
[6] U. Pison, W. Seeger, R. Buchhorn, T. Joka, M. Brand, U. Obertacke, H. Neuhof, K.P. Schmit-Nauerburg, Surfactant abnormalities in patients with respiratory failure after multiple trauma. Am. Rev. Respir. Dis. 140 (1989) 1033–1039.
[7] R.H. Notter, Z. Wang, Pulmonary surfactant: physical chemistry, physiology and replacement, Rev. Chem. Eng. 13 (1997) 1–118.
[8] J.F. Lewis, A.H. Jobe, Surfactant and the adult respiratory distress syndrome, Am. Rev. Respir. Dis. 147 (1993) 218–233.
[9] H.P. Haagsman, R.V. Diemel, Surfactant-associated proteins: functions and structural variation, Comp. Biochem. Physiol. 129 (2001) 91–108.
[10] L.M. Nogee, D.E. Demello, L.P. Dehner, H.R. Colten, Brief report—Deficiency of pulmonary surfactant protein-B in congenital alveolar proteinosis, N. Engl. J. Med. 328 (1993) 406–410.
[11] L.M. Nogee, G. Garnier, H.C. Dietz, L. Singer, A.M. Murphy, D.E. deMello, H.R. Colten, A mutation in the surfactant protein B gene responsible for fatal neonatal respiratory disease in multiple kindreds, J. Clin. Invest. 93 (1994) 1860–1863.
[12] J.C. Clark, S.E. Wert, C.J. Bachurski, M.T. Stahlman, B.R. Stripp, T.E. Weaver, J.A. Whitsett, Targeted disruption of the surfactant protein B gene disrupts surfactant homeostasis, causing respiratory failure in newborn mice, Proc. Natl. Acad. Sci. U. S. A. 92 (1995) 7794–7798.
[13] K. Tokieda, J.A. Whitsett, J.C. Clark, T.E. Weaver, K. Ikeda, K.B. McConnell, A.H. Jobe, M. Ikegami, H.S. Iwamoto, Pulmonary dysfunction in neonatal SP-B-deficient mice, Am. J. Physiol., Lung Cell. Mol. Physiol. 273 (1997) L875–L882.
[14] S.W. Glasser, T.R. Korfhagen, T. Weaver, T. Pilot-Matias, J.L. Fox, J.A. Whitsett, cDNA and deduced amino acid sequence of human pulmonary surfactant-associated proteolipid SPL(Phe), Proc. Nat. Acad. Sci. U. S. A. 84 (1987) 4007–4011.
[15] T. Curstedt, J. Johansson, J. Barros-Soderling, B. Robertson, G. Nilsson, V. Westberg, H. Jornvall, Low-molecular mass surfactant protein type I: the primary structure of a hydrophobic 8 kDa polypeptide with eight half-cystine residues, Eur. J. Biochem. 172 (1988) 521–525.
[16] S. Hawgood, M. Derrick, P. Poulain, Structure and properties of surfactant protein B, Biochim. Biophys. Acta 1408 (1998) 150–160.
[17] M. Andersson, T. Curstedt, H. Jörnvall, J. Johansson, An amphipathic helical motif common to tumourolytic polypeptide NK-lysin and pulmonary surfactant polypeptide SP-B, FEBS Lett. 362 (1995) 328–332.
[18] T.E. Weaver, J.J. Conkright, Functions of surfactant proteins B and C, Annu. Rev. Physiol. 63 (2001) 555–578.
[19] S. Zaltash, M. Palmblad, T. Curstedt, J. Johansson, B. Persson, Pulmonary surfactant protein B: a structural model and a functional analogue, Biochim. Biophys. Acta 1466 (2000) 179–186.
[20] S. Zaltash, W. Griffiths, D.C. Beck, C.-X. Duan, T.E. Weaver, J. Johansson, Membrane activity of (Cys48Ser) lung surfactant protein B increases with dimerization, Biol. Chem. 382 (2000) 933–939.
[21] R.S. Munford, P.O. Sheppard, P.J. O'Hara, Saposin-like proteins (SAPLIP) carry out diverse functions on a common backbone structure, J. Lipid Res. 36 (1995) 1653–1663.
[22] J.H. Power, I.R. Doyle, K. Davidson, T.E. Nicholas, Ultrastructural and protein analysis of surfactant in the Australian lungfish *Neoceratodus forsteri*: evidence for conservation of composition for 300 million years, J. Exp. Biol. 202 (1999) 2543–2550.
[23] E. Liepinsh, M. Andersson, J.-M. Ruysschaert, G. Otting, Saposin fold revealed by the NMR structure of NK-lysin, Nat. Struct. Biol. 4 (1997) 793–795.
[24] V.E. Ahn, K.F. Faull, J.P. Whitelegge, A.L. Fluharty, G.G. Prive, Crystal structure of saposin B reveals a dimeric shell for lipid binding, Proc. Natl. Acad. Sci. U. S. A. 100 (2003) 38–43.
[25] L.M. Gordon, S. Horvath, M.L. Longo, J.A.N. Zasadzinski, H.W. Taeusch, K. Faull, C. Leung, A.J. Waring, Conformation and molecular topography of the N-terminal segment of surfactant protein-B in structure-promoting environments, Protein Sci. 5 (1996) 1662–1675.
[26] L.M. Gordon, K.Y.C. Lee, M.M. Lipp, J.A.N. Zasadzinski, F.J. Walther, M.A. Sherman, A.J. Waring, Conformational mapping of the N-terminal segment of surfactant protein B in lipid using 13C-enhanced Fourier transform infrared spectroscopy, J. Pept. Res. 55 (2000) 330–347.

[27] K.Y. Lee, J. Majewski, T.L. Kuhl, P.B. Howes, K. Kjaer, M.M. Lipp, A.J. Waring, J.A.N. Zasadzinski, G.S. Smith, Synchrotron X-ray study of lung surfactant-specific protein SP-B in lipid monolayers, Biophys. J. 81 (2001) 572–585.
[28] B.N. Flanders, S.A. Vickery, R.C. Dunn, Imaging of monolayers composed of palmitic acid and lung surfactant protein B, J. Microsc. 202 (2001) 379–385.
[29] J.W. Kurutz, K.Y.C. Lee, NMR structure of lung surfactant peptide SP-B11–25, Biochemistry 41 (2002) 9627–9636.
[30] Y.N. Kaznessis, S. Kim, R.G. Larson, Specific mode of interaction between components of model pulmonary surfactants using computer simulations, J. Mol. Biol. 322 (2002) 569–582.
[31] J.A. Freites, Y. Choi, D.J. Tobias, Molecular dynamics simulations of a pulmonary surfactant protein B peptide in a lipid monolayer, Biophys. J. 84 (2003) 2169–2180.
[32] N. Biswas, S. Shanmukh, A. Waring, F.J. Walther, Z. Wang, Y. Chang, R.H. Notter, R.A. Dluhy, Structure and properties of phospholipid–peptide monolayers containing monomeric SP-B_{1-25}. I. Phases and morphology by epi-fluorescence microscopy, Biophys. Chem. 113 (2005) 223–232.
[33] S. Shanmukh, N. Biswas, A.J. Waring, F.J. Walther, Z.D. Wang, Y. Chang, R.H. Notter, R.A. Dluhy, Structure and properties of phospholipid–peptide monolayers containing monomeric SP-B_{1-25}. II. Peptide conformation by infrared spectroscopy, Biophys. Chem. 113 (2005) 233–244.
[34] E.J.A. Veldhuizen, A.J. Waring, F.J. Walther, J.J. Batenburg, L.M.G. van Golde, H.P. Haagsman, Dimeric N-terminal segment of human surfactant protein B (dSP-B_{1-25}) has enhanced surface properties compared to monomeric SP-B_{1-25}, Biophys. J. 79 (2000) 377–384.
[35] F.J. Walther, J.M. Hernandez-Juviel, L.M. Gordon, A.J. Waring, P. Stenger, J. Zasadzinski, Comparison of three lipid formulations for synthetic surfactant with a surfactant protein B analog, Exp. Lung Res. 31 (2005) 563–579.
[36] F.J. Walther, J.M. Hernandez-Juviel, L.M. Gordon, M.A. Sherman, A.J. Waring, Dimeric surfactant protein B peptide SP-B_{1-25} in neonatal and acute respiratory distress syndrome, Exp. Lung Res. 28 (2002) 623–640.
[37] F. Bringezu, J. Ding, G. Brezesinski, A.J. Waring, J. Zasadzinski, Influence of pulmonary surfactant protein B on model lung surfactant monolayers, Langmuir 18 (2002) 2319–2335.
[38] C.G. Fields, D.H. Lloyd, R.L. Macdonald, K.M. Ottenson, R.L. Noble, HBTU activation for automated Fmoc solid-phase peptide synthesis, Pept. Res. 4 (1991) 95–101.
[39] F. Picard, T. Buffeteau, B. Desbat, M. Auger, M. Pezolet, Quantitative orientation measurements in thin lipid films by attenuated total reflection infrared spectroscopy, Biophys. J. 76 (1999) 539–551.
[40] N.J. Harrick, Electric field strengths at totally reflecting interfaces, J. Opt. Soc. Am. 55 (1965) 851–857.
[41] U.P. Fringeli, H.H. Günthard, Membrane Spectroscopy, Springer Verlag, Berlin, 1981.
[42] M. Methot, F. Boucher, C. Salesse, M. Subirade, M. Pezolet, Determination of bacteriorhodopsin orientation in monolayers by infrared spectroscopy, Thin Solid Films 285 (1996) 627–630.
[43] R.D.B. Fraser, The interpretation of infrared dichroism in fibrous protein structures, J. Chem. Phys. 21 (1953) 1511–1515.
[44] T. Miyazawa, E.R. Blount, The infrared spectra of polypeptides in various conformations: Amide I and Amide II bands, J. Am. Chem. Soc. 83 (1961) 712–719.
[45] K.J. Rothschild, N.A. Clark, Polarized infrared spectroscopy of oriented purple membrane, Biophys. J. 25 (1979) 473–487.
[46] D. Marsh, Dichroic ratios in polarized Fourier transform infrared for nonaxial symmetry of beta-sheet structures, Biophys. J. 72 (1997) 2710–2718.
[47] U.P.a.G.H.H. Fringeli, Membrane Spectroscopy, Springer Verlag, Berlin, 1981.
[48] C.P. Lafrance, A. Nablet, R.E. Prud'homme, M. Pezolet, On the relationship between the order parameter <P2(cos theta)> and the shape of orientation distributions, Can. J. Chem. 73 (1995) 1497–1505.
[49] R. Chen, L. Li, Z. Weng, ZDOCK: An initial-stage protein docking algorithm, Proteins Struct. Funct. Genet. 52 (2003) 80–87.
[50] R. Koradi, M. Billeter, K. Wüthrich, MOLMOL: a program for display and analysis of macromolecular structures, J. Mol. Graph. 14 (1996) 51–55.
[51] W.L. DeLano, The PyMOL User's Manual, Delano Scientific, San Carlos, CA, 2002.
[52] P.R. Carey, Biochemical Applications of Raman and Resonance Raman Spectroscopies, Academic Press, New York, 1982.
[53] H.E. Van Wart, H.A. Scheraga, Raman spectra of strained disulfides—Effect of rotation about sulfur–sulfur bonds on sulfur–sulfur stretching frequencies, J. Phys. Chem. 80 (1976) 1823–1832.
[54] H.E. Van Wart, H.A. Scheraga, Raman spectra of cystine-related disulfides—Effect of rotational isomerism about carbon–sulfur bonds on sulfur–sulfur stretching frequencies, J. Phys. Chem. 80 (1976) 1812–1823.
[55] H. Sugeta, A. Go, T. Miyazawa, S–S And C–S stretching vibrations and molecular conformations of dialkyl disulfides and cystine, Chem. Lett. (1972) 83–87.
[56] A.T. Tu, Peptide backbone conformation and microenvironment of protein side chains, in: R.J.H. Clark, R.E. Hester (Eds.), Spectroscopy of Biological Systems, John Wiley and Sons, Ltd., London, 1986, pp. 47–112.
[57] M.N. Siamwiza, R.C. Lord, M.C. Chen, T. Takamatsu, I. Harada, H. Matsuura, T. Shimanouchi, Interpretation of doublet at 850 and 830 cm^{-1} in Raman-spectra of tyrosyl residues in proteins and certain model compounds, Biochemistry 14 (1975) 4870–4876.
[58] S. Ikeda, E.C.Y. Li-Chan, Raman spectroscopy of heat-induced fine-stranded and particulate beta-lactoglobulin gels, Food Hydrocoll. 18 (2004) 489–498.
[59] M.C. Chen, R.C. Lord, R. Mendelsohn, Laser-excited Raman spectroscopy of biomolecules. 4. Thermal denaturation of aqueous lysozyme, Biochim. Biophys. Acta 328 (1973) 252–260.
[60] N.T. Yu, Comparison of protein structure in crystals, in lyophilized state, and in solution by laser Raman scattering. 3. Alpha-lactalbumin, J. Am. Chem. Soc. 96 (1974) 4664–4668.
[61] A.T. Tu, B.H. Jo, N.T. Yu, Laser Raman spectroscopy of snake venom neurotoxins—Conformation, Int. J. Pept. Protein Res. 8 (1976) 337–343.
[62] H. Ishizaki, R.H. McKay, T.R. Norton, K.T. Yasunobu, J. Lee, A.T. Tu, Conformational studies of peptide heart stimulant anthopleurin-A—Laser Raman, circular-dichroism, fluorescence spectral studies, and Chou-Fasman calculations, J. Biol. Chem. 254 (1979) 9651–9656.
[63] R.C. Lord, N.T. Yu, Laser-excited Raman spectroscopy of biomolecules. 1. Native lysozyme and its constituent amino acids, J. Mol. Biol. 50 (1970) 509–513.
[64] R.C. Lord, N.T. Yu, Laser-excited Raman spectroscopy of biomolecules. 2. Native ribonuclease and alpha-chymotrypsin, J. Mol. Biol. 51 (1970) 203–207.
[65] M. Hayashi, T. Shimanouchi, S. Mizushima, Raman and infrared spectra of 2-thiabutane, J. Chem. Phys. 26 (1957) 608–612.
[66] E.B. Carew, I.M. Asher, H.E. Stanley, Laser Raman spectroscopy—New probe of myosin substructure, Science 188 (1975) 933–936.
[67] I. Harada, H. Takeuchi, Raman and ultraviolet resonance Raman spectra of proteins and related compounds, in: R.J.H. Clark, R.E. Hester (Eds.), Spectroscopy of Biological Systems, vol. 13, John Wiley and Sons, Chichester, 1986, pp. 113–176.
[68] Y.D. Wang, K.M.K. Rao, E. Demchuk, Topographical organization of the N-terminal segment of lung pulmonary surfactant protein B (SP-B_{1-25}) in phospholipid bilayers, Biochemistry 42 (2003) 4015–4027.
[69] U.P. Fringeli, H.H. Günthard, Infrared membrane spectroscopy, in: E. Grell (Ed.), Membrane Spectroscopy, vol. 31, Springer-Verlag, Berlin, 1981, pp. 270–332.
[70] J.E. Baatz, B. Elledge, J.A. Whitsett, Surfactant protein SP-B induces ordering at the surface of model membrane bilayers, Biochemistry 29 (1990) 6714–6720.
[71] C.G. Cochrane, S.D. Revak, Pulmonary surfactant protein B (SP-B): structure–function relationships, Science 254 (1991) 566–568.
[72] T. Curstedt, J. Johansson, P. Persson, A. Eklund, B. Robertson, B. Lowenadler, H. Jornvall, Hydrophobic surfactant-associated polypeptides: SP-C is a lipopeptide with two palmitoylated cysteine residues, whereas SP-B lacks covalently linked fatty acyl groups, Proc. Nat. Acad. Sci. U. S. A. 87 (1990) 2985–2990.

[73] J. Johansson, T. Curstedt, H. Jornvall, Surfactant protein B—Disulfide bridges, structural properties, and Kringle similarities, Biochemistry 30 (1991) 6917–6921.
[74] A. Takahashi, A.J. Waring, J. Amirkhanian, B. Fan, W. Taeusch, Structure–function relationships of bovine pulmonary surfactant proteins: SP-B and SP-C, Biochim. Biophys. Acta 1044 (1990) 43–49.
[75] H. Sugeta, A. Go, T. Miyazawa, Vibrational spectra and molecular conformations of dialkyl disulfides, Bull. Chem. Soc. Jpn. 46 (1973) 3407–3411.
[76] H.E. Van Wart, F. Cardinaux, H.A. Scheraga, Low frequency Raman spectra of dimethyl, methyl ethyl, and diethyl disulfides, and rotational isomerization about their carbon–sulfur bonds, J. Phys. Chem. 80 (1976) 625–630.